Impact of composition modification induced by ion beam Coulomb-drag effects on the nanoindentation hardness of HT9

Gigax, Jonathan Gregory
Kim, Hyosim
Aydogan, Eda
Price, Lloyd M
Wang, Xuemei
Maloy, Stuart Andrew
Garner, Frank A
Shao, Lin

To be published in: Nuclear Instruments and Methods in Physics Research Section B: Beam Interactions with Materials and Atoms

DOI to publisher's version: 10.1016/j.nimb.2018.12.051

Impact of composition modification induced by ion beam Coulomb-drag effects on the nanoindentation hardness of HT9

Jonathan G. Gigax[a,*], Hyosim Kim[b], E. Aydogan[c], L. M. Price[b], X. Wang[b], S. A. Maloy[a], F. A. Garner[b], and L. Shao[b]

[a] Los Alamos National Lab, Los Alamos, NM 87545

[b] Department of Nuclear Engineering, Texas A&M University, College Station, TX 77843

[c] Integrated Manufacturing Center, Sabanci University, Istanbul, Turkey 34906

*Corresponding Author: email address: jgigax@lanl.gov

Abstract

Accelerator-based ion irradiation is commonly used to simulate neutron damage, in lieu of neutron irradiation due to limited availability of fast flux facilities and little to no activation of the samples. Neutron atypical effects, however, must be recognized and their impact minimized in order to achieve the most accurate microstructural evolution under ion bombardment. Mechanical property changes, which arise from the synergy of numerous radiation-induced changes, are especially susceptible to these neutron atypical effects. Of these effects, a recently studied neutron atypical effect, arising from Coulomb-drag of vacuum contaminants and subsequent compositional alteration, was shown to substantially suppress swelling. Through the use of an ion beam filtering system, the resulting void swelling was shown to closely match neutron irradiation data. In this study, the impact of compositional modification via Coulomb-drag on the mechanical property changes is examined through the use of nanoindentation on a ferritic/martensitic alloy, HT9, irradiated with and without the use of the ion beam filtering system.

Keywords: ion beam processing; ion implantation; nanoindentation

IBMM 2018 Abstract Number 46

1. Introduction

The use of ion irradiation as a surrogate for neutron irradiation was largely spurred by the lack of fast flux facilities and the long durations needed to achieve damage levels expected in next-generation fast reactors. Ion irradiation studies, as a surrogate to neutron irradiation, have shown the ability to reproduce the steady-state swelling rates of 0.2 %/dpa and 1 %/dpa for ferritic/martensitic (F/M) and austenitic alloys obtained from neutron irradiations, respectively [1,2].

Unlike fast neutron irradiation, where dose gradients are minimal across several hundred micrometers, the relatively short range of ions typically used for damage studies results in strong dose rate gradients over a few micrometers near the ion-incident surface. This gives rise to a number of neutron atypical effects [3-6]. As a result, the microstructure in the near surface region must be clean and relatively free of preparation-induced defects in order to accurately capture the bulk response of the system under irradiation. The limited irradiation volume imposes severe restrictions on the application of macroscale mechanical testing. Thus, nano- and microscale mechanical tests are needed to accurately evaluate radiation-induced mechanical property changes.

The possibility of compositional modification (i.e. contamination) during ion irradiation has been the subject of discussion but was only very recently addressed [7-9]. It was discovered that vacuum contaminants, such as carbon- and oxygen-rich molecules and nitrogen, can be entrained into the beam and delivered onto the ion-irradiated area [7]. A simple solution was devised by implementing cold traps to getter charge-neutral molecules while a series of bending magnets was set to deflect the beam through small angles [8]. Since entrained contaminants typically possess a lower mass and energy than the primary ion beam, these contaminants are deflected through even larger angles and effectively removed from the ion beam.

The impact of this neutron atypical effect on void swelling in HT9 was studied previously and was shown to be suppressed effectively by the ion beam filtering system [8]. However, the mechanical property changes arising from this compositional modification alone have not yet been examined. If the void swelling behavior exhibited dramatic differences between a filtered and unfiltered irradiation, then it is reasonable to expect that the mechanical property changes will be influenced similarly. In this study, we utilize nanoindentation to assess the hardness changes in HT9 irradiated with and without the ion beam filter to better understand the potential impact ion beam-induced compositional modifications may have on the mechanical properties after irradiation.

2. Experimental Methods

HT9, with a composition given in Table 1, was heat treated by annealing at 1040 °C for 30 min and air cooled, followed by tempering at 760 °C for 1 h and air cooling. Specimens 3 millimeters in diameter were sectioned and polished to 4000 grit SiC paper. The HT9 disks were jet electropolished using a solution of 5 vol.% perchloric acid and 95 vol.% methanol at -40 °C and 20 V to remove any damage layer from mechanical polishing.

The HT9 was irradiated with 3.5 MeV Fe^{2+} ions at 450 °C. To avoid effects of void swelling suppression from rastering, a static ion beam was defocused over the sample area to give a time averaged dpa rate of 1.74×10^{-3} dpa/s [4]. Two sets of specimens were compared in this study. The first set of HT9 disks was irradiated to 200, 400, and 600 peak dpa as calculated using the Kinchin-Pease option of SRIM-2013 with a 40 eV displacement energy [10,11]. The second set of specimens was irradiated to 200, 400, 600, and 800 peak dpa using a newly developed ion beam filtering systems to remove contaminants entrained by the ion beam [7,8].

Nanoindentation was performed with a Hysitron TI-950 Triboindenter using a low load transducer equipped with a diamond Berkovich tip. Specimens were loaded at a constant rate up to a maximum force of 10 mN over 5 s, held at 10 mN for 2 s, and then unloaded at a constant rate over 5 s. Random locations on the sample with 6-20 indents were made to better capture the change in hardness after irradiation. Secondary ion mass spectroscopy (SIMS) depth profiles of carbon, oxygen, and nitrogen were obtained using a Physical Electronics Model 6600 SIMS System with a 4 keV Cs beam. We note that one sample where SIMS was performed, fewer indents were made due to the significantly reduced area from the analysis. Transmission electron microscopy (TEM) specimens were prepared using a TESCAN Lyra focused ion beam mill using a technique described elsewhere [12]. Scanning transmission electron microscopy (STEM) high-angle annular dark-field (HAADF), and bright field images were obtained using an FEI Tecnai F20 Super Twin operated at 200 kV. To calculate void swelling, TEM lamella thicknesses were measured using a conventional technique using electron energy loss spectroscopy.

Table 1 – Composition of the HT9 heat used in the present study.

	Fe	C	Cr	Mo	Si	Mn	Ni	V	W
wt. %	bal.	0.21	12.5	1.1	0.29	0.41	0.6	0.3	0.51

3. Results

Fig. 1a shows a typical nanoindentation load-depth plot of an unirradiated HT9 and HT9 irradiated to 600 peak dpa with and without a filter. At a maximum load of 10 mN, the Berkovich tip did not indent beyond a depth of 400 nm. Although higher loads can be applied, a relatively low load was selected to ensure that the material volume contributing to the hardness signal remained largely within the ion irradiated region, while avoiding hardening from size effects at shallower depths [13].

Fig. 1b provides a comparison of the nanoindentation hardness extracted from the load-displacement curves using the Oliver-Pharr method [14]. The unirradiated HT9 had a measured hardness of 3.6 ± 0.13 GPa. Without filtering, the hardness was observed to increase monotonically with increasing damage level up to 600 peak dpa where the hardness was measured to be 4.8 ± 0.35 GPa, a 33% increase in hardness above that of the unirradiated HT9.

The HT9 irradiated with a filter displayed a more complex behavior (Fig. 1b). The hardness was observed to increase to 4.3 ± 0.15 GPa after 200 peak dpa, closely matching that observed in the unfiltered irradiation. However, the hardness of the HT9 decreased to 4.2 ± 0.3 GPa at 400 peak dpa and further to 3.9 ± 0.3 at 600 peak dpa. The hardness at 800 peak dpa (4.0 ± 0.4 GPa) was not significantly different than that measured at 600 peak dpa.

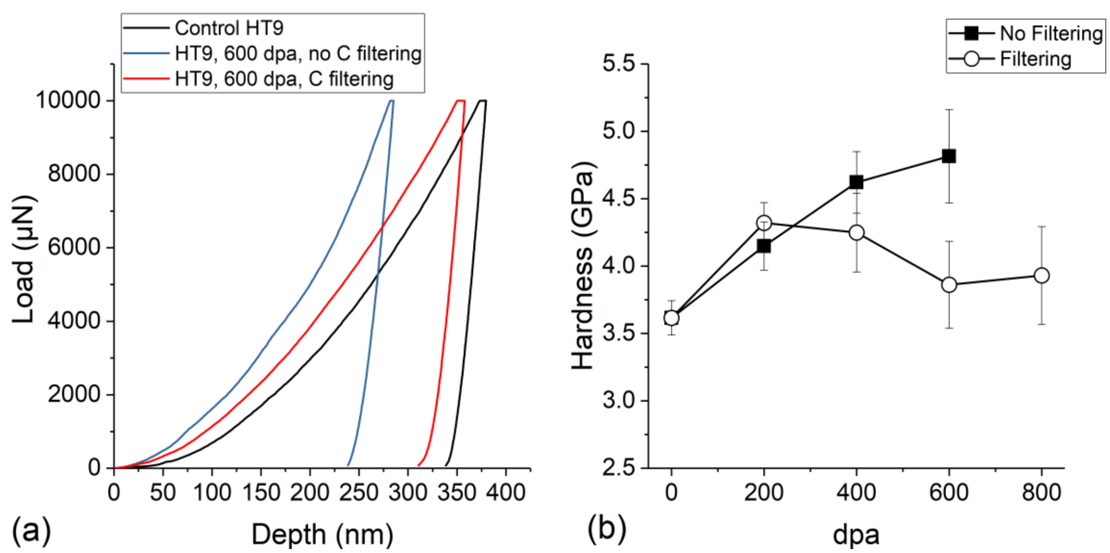

Figure 1 - (a) Typical load-depth plots for HT9 irradiated to 600 peak dpa and (b) comparison of the average hardness of the HT9 after irradiation with and without filtering.

In order to understand the differences in hardness change with damage level, we focused our analysis on two radiation-induced phenomena which showed large differences between the two irradiation sets: carbide precipitation and void swelling. Fig. 2 provides the STEM and dark-field micrographs of the unirradiated HT9 and HT9 irradiated to 200 peak dpa with and without filtering. Fig. 2a shows the fine lathe structure of the unirradiated HT9 and the large carbides along grain boundaries (noted by black arrows), previously identified as $M_{23}C_6$ [8]. Within grains, there is no evidence of significant carbide precipitation prior to irradiation. After irradiation to 200 peak dpa, small carbides were observed to appear in both the filtered and unfiltered HT9 specimens (Fig. 2d and 2e). Both irradiated specimens contained carbides of similar density and size, with a carbide volume fraction of 0.004 and 0.007 for the unfiltered and filtered specimens, respectively. Significant void swelling was not observed at this damage level with only a few voids less than 25 nm in diameter observed in both specimens. The measured void swelling in either specimen was ~0.03%.

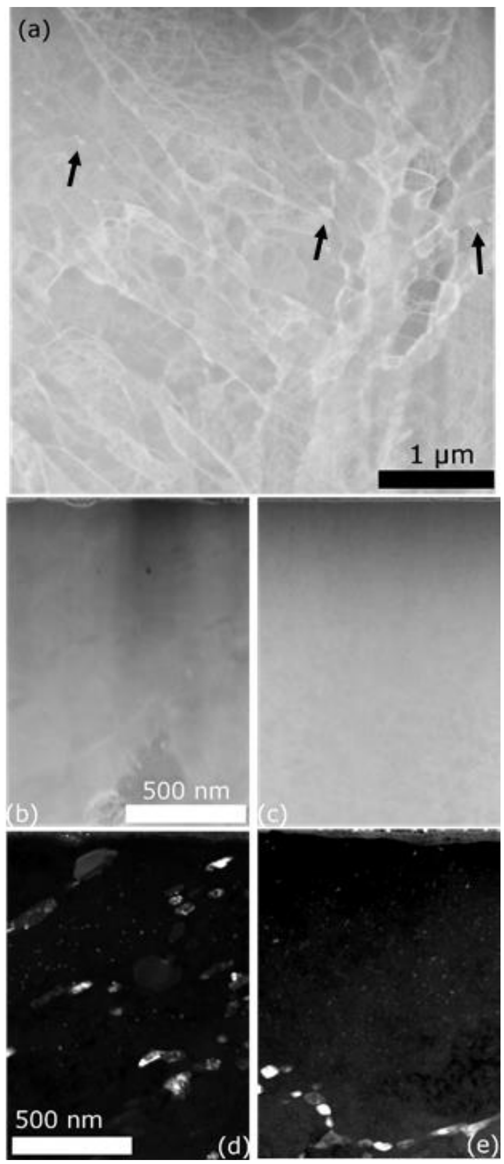

Figure 2 – Typical STEM micrographs of (a) unirradiated HT9 and HT9 irradiated to 200 peak dpa (b) without and (c) with filtering, and corresponding dark field images of HT9 irradiated (d) without and (e) with filtering. Black arrows in (a) mark grain boundary carbides.

The largest difference in nanoindentation hardness in the irradiated HT9 was observed at 600 peak dpa. At this damage level, the hardness in the unfiltered HT9 was ~25% higher than in the filtered HT9. SIMS analysis performed on the specimens irradiated at this damage level is provided in Figs. 3a-c, with a plot of the calculated dpa and ion range curves from SRIM provided as reference in Fig. 3d. The average amount of carbon in the irradiation volume in the filtered HT9 was measured to be ~1.5 at. %, agreeing closely with the SIMS measured value of 1.3 at. % in the unirradiated HT9. The average carbon concentration in the unfiltered HT9 was measured to be 4 at. %. Since the average carbon concentration is several times larger than the solubility limit of carbon in bcc Fe, it is expected that the unfiltered HT9 should contain a larger carbide volume fraction than filtered HT9 at this damage level.

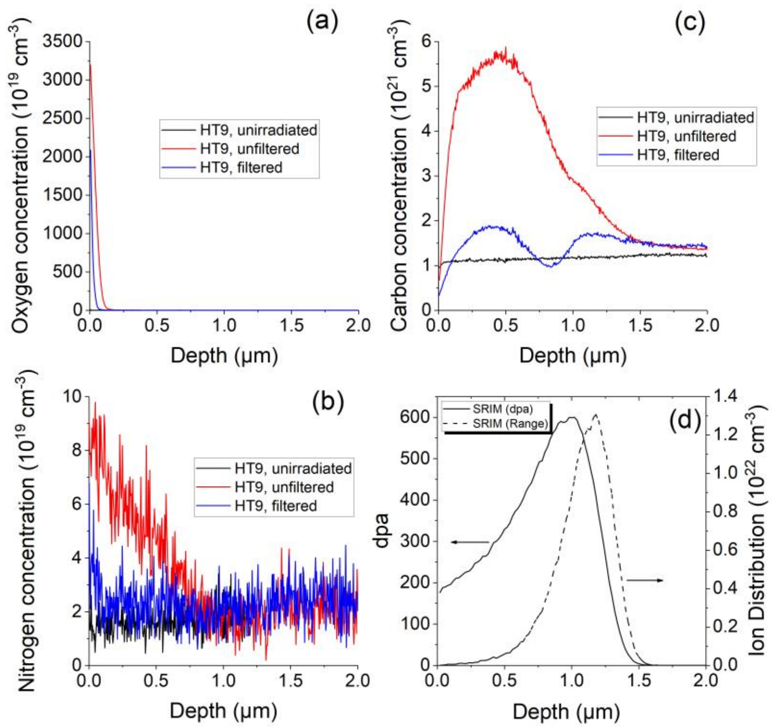

Figure 3 – (a) Oxygen, (b) nitrogen, and (c) carbon comparison for unirradiated HT9 and HT9 irradiated to 600 peak dpa with and without filtering. (d) SRIM dpa and range curves.

From the STEM and dark-field TEM micrographs of HT9 irradiated to 600 peak dpa in Figs. 4, there are two important observations to be made with respect to voids and carbide precipitates in the respective specimens. The carbide density and size observed in the irradiated region of the unfiltered HT9 (Fig. 4c) is clearly larger than that in the filtered HT9 (Fig. 4d). The average carbide volume fraction in the unfiltered HT9 was calculated to be ~0.12, an order of magnitude higher than the 0.014 measured in the filtered HT9 specimen, in agreement with the conclusion derived from SIMS (Fig. 3a). From Figs. 4a and 4b the overall void size and density of the HT9 irradiated with the filtering system was higher than that of the HT9 irradiated without the filter.

The resulting void swelling in the filtered specimen reached ~1.3%, nearly an order of magnitude higher than that of the unfiltered HT9 at ~0.19%.

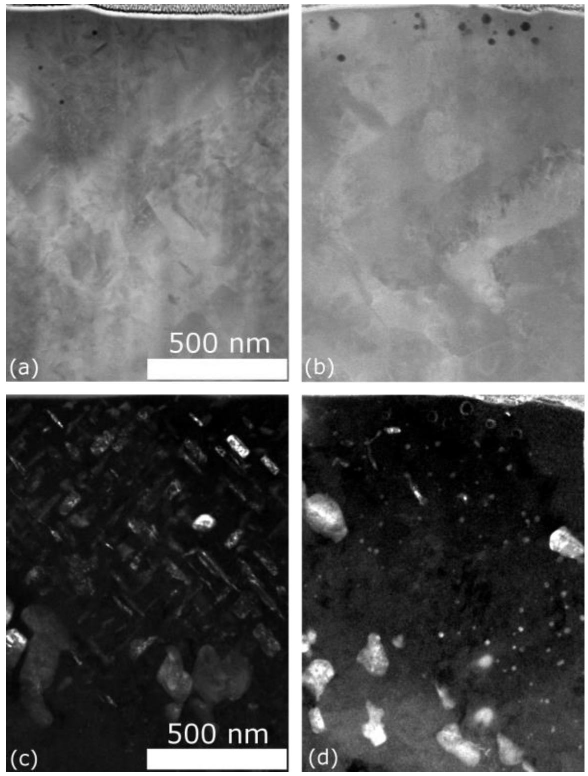

Figure 4 – Typical STEM micrographs of HT9 irradiated to 600 peak dpa (a) without and (b) with filtering and corresponding dark field images of HT9 irradiated (c) without and (d) with filtering.

4. Discussion

From nanoindentation and microscopic investigations, there are two notable developments in the microstructure that echo the conclusions made in our previous study [8]. Without a filtering system, the microstructure of HT9 developed a high density of large carbides with little or no void swelling, giving rise to an ever-increasing hardness with damage level. The implementation of a filtering system resulted in the development of small carbides at low doses, and large voids and void swelling at higher damage levels.

From a quick glance, it is convenient to attribute the difference in hardness to the differences in both carbide precipitation and void swelling. Despite the large differences in void swelling at 600 peak dpa, neither specimens exhibited swelling to levels greater than a few percent. Furthermore, the large differences in carbide precipitation, especially at 600 peak dpa, contrast to the comparatively smaller difference in hardness measured at this damage level. Is it reasonable to expect that swelling of this amount should induce softening of the material? Moreover, does a conventional model of precipitate hardening adequately explain the apparent discrepancy between the difference in carbide precipitation and measured hardness?

Carbon solution strengthening is a well-known technique to improve the wear resistance of materials through the introduction of interstitial carbon to the microstructure. At concentrations above the 0.02 wt. % (~1 at. %) limit in body-centered cubic Fe systems, carbon precipitates out of solution as a precipitate whose composition and structure are determined, in part, by the amount of excess carbon in the system. Several types of carbides were previously observed in this system after irradiation, including $M_{23}C_6$, M_7C_3, and M_3C [8]. Carbides possess a higher hardness than the tempered martensite matrix, typically greater than 15 GPa, resulting in an overall hardening effect from carbide precipitation [15]. It is assumed that the precipitation of carbides does not reduce the amount of carbon in solid solution.

The change in hardness arising from carbide precipitation and growth can be calculated using the dispersion barrier hardening (DBH) model [16],

$$\Delta\sigma_c = 0.8M\alpha Gb/\lambda$$

where M is the Taylor factor and measured to be ~3 for bcc polycrystalline metals [17], α is the barrier strength coefficient, G is the shear modulus of the matrix, b is the magnitude of Burger's vector (0.248 nm for {111}[110]), and λ is the mean free path between precipitates. For the purpose of estimating the hardness contribution, we have assumed the barrier strength coefficient to be 0.5 and the shear modulus to be 60 GPa. Calculation of mean free path for precipitates with high aspect ratios cannot be accurately made by simplifying them as spherical precipitates, even for estimates. The mean free path can, however, be calculated using a similar formalism derived for spherical precipitates with considerations made by Sonderegger and Kozeschnik [18],

$$\lambda = \sqrt{\frac{\ln(3)}{2\pi\sum_i n_{V,i}n_i} + (2r_A)^2} - 2r_A$$

where

$$r_A = \sqrt{\frac{2}{3} \times \frac{\sum_i n_{V,i} n_i^2}{\sum_i n_{V,i} n_i}}$$

and r_A is the mean radius of the intersection area of the precipitate and slip plane. For a given particle type i, $n_{V,i}$ is the density of precipitates, and n_i is defined as the distance from the center of a precipitate to the slip plane when the plane just touches the precipitate. For particles with half-axes aligned to (100) in a bcc system, n_i can be calculated by,

$$n_i = \frac{2a_i^2 + c_i^2}{2}$$

where a_i and c_i are the half-axes of the precipitate.

The other phenomenon under consideration, void swelling, is a well-studied life limiting phenomenon occurring in nuclear reactors, specifically in fast reactors [19]. At small sizes, both voids and He bubbles have been observed to increase hardness of irradiated steels [20,21]. The hardening from voids can be calculated from

$$\Delta\sigma_V = M\alpha Gb\sqrt{N \times d}$$

Where α is a constant measured to be 0.38 for polycrystalline iron [22], N is the density of voids, and d is the size of the voids. The equation above suggests that the change in hardness should increase monotonically with increasing void size and density. However, at higher swelling values, starting at ~5% in stainless steels, the hardness of irradiated steels was observed to decrease precipitously, as observed by uniaxial tensile and ring pull tests [23]. The underlying cause of the drop was attributed to the fact that significant void swelling reduces the shear modulus which, in turn, lowers the barrier strength of defect sinks. The net effect is a softening and embrittlement of the material.

Figs. 5a and 5b provide a comparison of the hardness changes observed in the HT9 irradiated without and with a filter, respectively. The calculated contributions to hardness from the carbides and voids are also provided in each plot. In the unfiltered irradiation (Fig. 5a), it is clear that the hardening contribution from voids is not significant. At low doses, the hardening contribution from carbides is similar to the hardness change measured in the irradiated specimens, suggesting that the carbon precipitates play a dominant role in the change in mechanical response. At higher doses, however, the estimated hardening from carbide growth exceeds the measured hardness change in the irradiated HT9. From the present data, it is difficult to attribute a single source to the observed change. It is possible that the previous assumption of a constant concentration of carbon in solid solution is incorrect, and that, in the extreme, all of the carbon in solid solution precipitated out, resulting in a softening of the material. On the other hand, more complex carbide behavior or carbide-dislocation interaction under indentation (e.g. fracture or dissolution) may also serve to reduce the effectiveness of these carbides as barriers to dislocation motion. We note that while there are other sources of hardening in the material under irradiation, such as dislocation loop formation and densification of the dislocation network, these do not resolve the large discrepancy in expected hardness change.

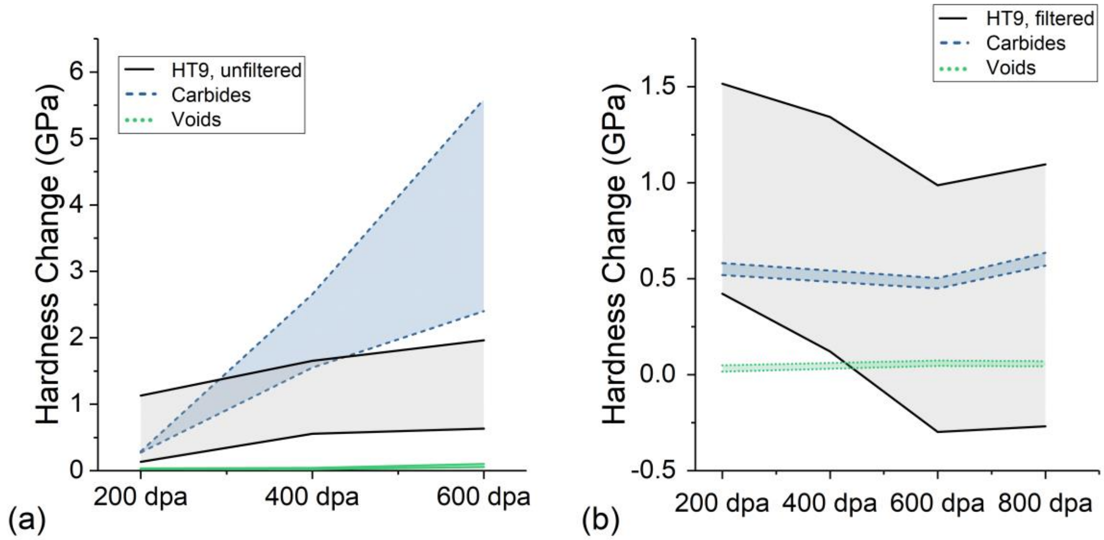

Figure 5 – Measured hardness change in HT9 and calculated hardening from carbide and void formation for the (a) unfiltered and (b) filtered HT9 irradiations. The shaded region bound by solid or dashed lines represents one standard deviation from the mean of hardness values.

The hardness change observed in the filtered HT9 irradiation (Fig. 5b) shows agreement with the estimated hardening from carbide precipitation. Despite more void swelling, hardening from voids was not observed to be a major contribution. While carbides appear to match the average change in hardness of HT9, the softening observed from 200 peak dpa to 600 peak dpa is not accounted for by these two sources alone. One possibility may be that since nanoindentation is a more localized test compared to bulk mechanical tests (i.e. tensile or compression tests), the localized void swelling of ~3% near the surface may serve to soften the material, rather than harden. However, we must also acknowledge that a thin oxide layer was observed after irradiation with a thickness of ~20 nm measured by TEM, but the filtered irradiation showed a lesser oxide growth with a thickness of ~5 nm. The differences in oxide layer growth may also influence the hardness differences.

For the purpose of discussion, we consider the possibility that at a high carbide volume fraction, the DBH model may not appropriately describe the hardening of the system. At high carbide volume fractions, the calculated hardness can surpass an upper limit of the harder phase since $\Delta\sigma_c \propto 1/\lambda$. In this case, a simpler interpretation using the rule of mixtures (ROM) may lead to a better fit of the data. The upper limit to the hardness of a mixture can be described by

$$H' = f_c H_c + f_m H_m$$

Where H' is the hardness of the composite under iso-strain conditions on both phases, f_c and f_m are the volume fractions of the carbide and matrix, and H_c and H_m are the hardnesses of the carbide and matrix, respectively. The lower limit to the hardness of a composite is

$$H'' = (\frac{f_c}{H_c} + \frac{f_m}{H_m})^{-1}$$

where H'' is the hardness of the composite under iso-stress conditions on both phases. Figs. 6 compare the measured hardness of the unfiltered HT9 (Fig. 6a) and filtered HT9 (Fig. 6b) with the estimates dervied from the rule of mixtures.

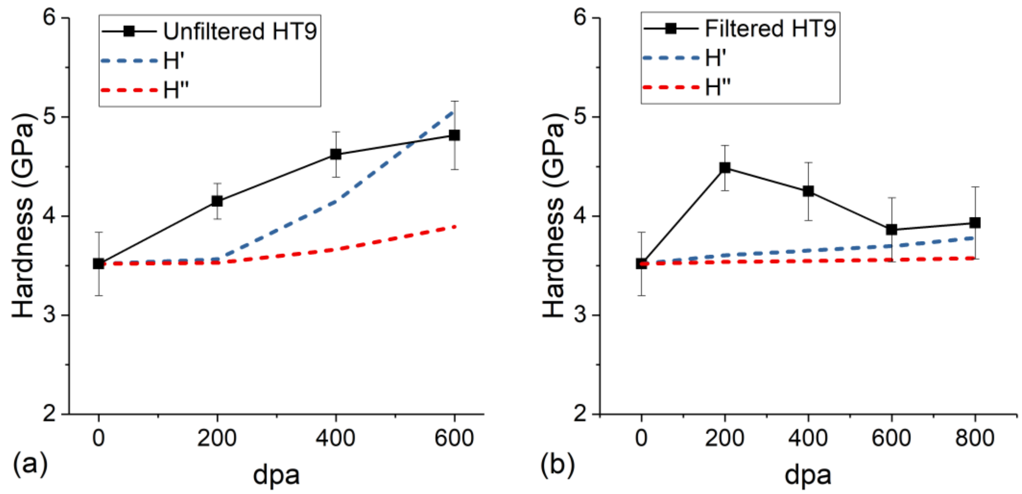

Figure 6 – Measured hardness of HT9 and predicted ROM hardness for the (a) unfiltered and (b) filtered HT9 irradiations. H' and H" are the hardness under iso-strain and iso-stress conditions, respectively.

At low damage levels, ROM hardness estimates do not appropriately predict the hardness of the irradiated HT9. The DBH model (Fig. 5) provides a much closer prediction. At higher damage levels starting at 400 dpa in the unfiltered and 600 dpa in the filtered irradiations, the upper limit of hardness calculated by the rule of mixtures closely matches the expected results.

5. Conclusion

An HT9 heat was ion irradiated at 450 °C to damage levels of 200, 400, and 600 peak dpa without beam filtering, and 200, 400, 600, and 800 peak dpa with beam filtering, respectively. Nanoindentation hardness mesaurements made using a Berkovich tip showed a monotonically increasing hardness for the unfiltered HT9 reaching a hardness value of ~4.8 GPa. Hardness measurements on the filtered HT9 showed an initial increase in hardness up to 400 peak dpa, followed by a decrease to a hardness value of ~4.0 GPa at 600 and 800 peak dpa. The major difference in hardness at 600 peak dpa was thought to arise from the difference in carbon concentration and, subsequently, the carbide volume fraction. Calculation of the hardness changes due to void swelling and carbide growth reproduced the observed behavior but were not able to accurately predict the hardness when carbides comprise a significant volume fraction of the material (~40 vol.%). A simple rule-of-mixtures calculation showed better agreement at these carbide volume fractions. The present work clearly shows that ion irradiation must be conducted cleanly and with beam contamination in mind. Without a technique or system to filter contaminants in the beam, both the microstructure and, consequently, the mechanical properties of the irradiated system will be subject strongly to a neutron atypical effect. This, in turn, limits its value in comparisons with other ion irradiated and neutron irradiated alloys.

6. Acknowledgements

The authors would like to acknowledge funding support by the U.S. Department of Energy, NEUP program [grant number DE-NE0008297].

7. References

1. F. A. Garner, L. Shao, M. B. Toloczko, S. A. Maloy, V. N. Voyevodin, Use of self-ion bombardment to study void swelling in advanced radiation-resistant alloys, Proceedings of the 17th International Conference on Environmental Degradation of Materials in Nuclear Power Systems - Water Reactors; 2015 August; Ontario, Canada.
2. V. Bryk, O. Borodin, A. Kalchenko, V. Voyevodin, V. Ageev, A. Nikitina, V. Novikov, V. Inozemtsev, F. A. Garner, Ion issues on irradiation behavior of structural materials at high doses and gas concentrations, Proceedings of the Accelerator Applications 2013; 2013 August 5-8; Bruges, Belgium.
3. L. Shao, C. C. Wei, J. G. Gigax, A. Aitkaliyeva, D. Chen, B. H. Sencer, F. A. Garner, Effect of defect imbalance on void swelling distributions produced in pure iron by 3.5 MeV self-ions, J Nucl Mater. 453 (2014) 176-181.
4. J. G. Gigax, E. Aydogan, T. Chen, D. Chen, L. Shao, Y. Wu, W. Y. Lo, Y. Yang, F.A. Garner, The influence of ion beam rastering on the swelling of self-ion irradiated pure iron at 450°C, J. Nucl. Mater. 465 (2015) 343-348.
5. F. A. Garner, G. L. Wire, E. R. Gilbert, Stress Effects in Ion-Bombardment Experiments. Proceedings of the Radiation Effects and Tritium Technology for Fusion Reactors; 1975 October 1-3; Gatlinburg (TN).
6. F.A. Garner, Impact of the Injected Interstitial on the Correlation of Charged Particle and Neutron-Induced Radiation Damage, J. Nucl. Mater. 117(1983) 177-197.
7. L. Shao, J. G. Gigax, D. Chen, Hyosim Kim, F. A. Garner, J. Wang, M. B. Toloczko, Standardization of accelerator irradiation procedures for simulation of neutron induced damage in reactor structural materials, Nucl. Instrum. Meth. Phys. Res. B 490 (2017) 251-254.
8. J. G. Gigax, Hyosim Kim, E. Aydogan, F. A. Garner, S. A. Maloy, L. Shao, Beam-contamination-induced compositional alteration and its neutron-atypical consequences in ion simulation of neutron-induced void swelling, Mater. Res. Lett. 5 (2017) 478-485.
9. G. Was, S. Taller, Z. Jiao, A. M. Monterrosa, D. Woodley, D. Jennings, T. Kubley, F. Naab, O. Toader, E. Uberseder, Resolution of the carbon contamination problem in ion irradiation experiments, Nucl. Instrum. Meth. Phys. Res. B 412 (2017) 58-65.
10. J.F. Ziegler, M.D. Ziegler, J.P. Biersack, RIM – The stopping and range of ions in matter (2010), Nucl. Instr. Methods Phys. Res. B 268.
11. R. Stoller, M.B. Toloczko, G.S. Was, A.G. Certain, S. Dwaraknath, F.A. Garner, On the use of SRIM for computing radiation damage exposure, Nucl. Meth. Phys. Res. Sect. B 310, (2013) 75-80.
12. J. G. Gigax, T. Chen, Hyosim Kim, J. Wang, L.M. Price, E. Aydogan, S. A. Maloy, D. K. Schreiber, M. B. Toloczko, F. A. Garner, L. Shao, Radiation response of alloy T91 at damage levels up to 1000 peak dpa, J. Nucl. Mater. 482 (2016) 257-265.
13. A. A. Elmustafa and D. S. Stone, Nanoindentation and the indentation size effect: Kinetics of deformation and strain gradient plasticity, J. Mech. Phys. Sol. 51 (2003) 357-381.
14. W. C. Oliver and G. M. Pharr, An improved technique for determining hardness and elastic modulus using load and displacement sensing indentation experiments, J. Mater. Res. 7 (1992) 1564-1583.
15. D. Casellas, J. Caro, S. Molas, J. M. Prado, I. Valls, Fracture toughness of carbides in tool steels evaluated by nanoindentation, Acta Mater. 55 (2007) 4277-4286.

16. S.J. Zinkle, Y. Matsukawa, Observation and analysis of defect cluster production and interactions with dislocations, J. Nucl. Mater. 329-333 (2004) 88-96.
17. R.E. Stoller, S.J. Zinkle, On the relationship between uniaxial yield strength and resolved shear stress in polycrystalline materials, J. Nucl. Mater. 283-287 (2000) 349-352.
18. B. Sonderegger and E. Kozeschnik, Particle strengthening in fcc crystals with prolate and oblate precipitates, Scripta Mater. 66 (2012) 52-55.
19. F.A. Garner, Radiation Damage in Austenitic Steels, in Konings, R.J.M., (ed.) Comprehensive Nuclear Materials, Volume 4, (2012) pp. 33-95, Elsevier.
20. F. A. Garner, M. L. Hamilton, N. F. Panayotou, G. D. Johnson, The microstructural origins of yield strength changes in AISI 316 during fission or fusion irradiation, J. Nucl. Mater. 103 & 104 (1981) 803-808.
21. G. E. Lucas, The evolution of mechanical property change in irradiated austenitic stainless steels, J. Nucl. Mater. 206 (1993) 287-305.
22. A.S. Keh, Direct observation of imperfections in crystals, in: J.B. Newkirk, J.H. Wernick (Eds.), Conference Proceedings on Direct Observations of Imperfections in Crystals, Interscience, New York, 1962, pp. 213-233.
23. V. S. Neustroev and F. A. Garner, Severe Embrittlement of Neutron Irradiated Austenitic Steels Arising from High Void Swelling, J. Nucl. Mater. 378 (2008) 327-332.